J Mater Sci (2009) 44:5256–5262
DOI 10.1007/s10853-009-3537-1

FERROELECTRICS

Effect of uniaxial stress on the electromechanical properties in ferroelectric thin films under combined loadings

Hai-Xia Cao · Veng Cheong Lo · Zhen-Ya Li

Received: 26 February 2009 / Accepted: 30 April 2009 / Published online: 27 May 2009

Abstract The electromechanical properties of ferroelectric thin films under an alternating electric field and a static uniaxial compressive stress are investigated using the modified planar four-state Potts model. To implement the electromechanical properties and the coupling of the electrical and mechanical response, the mechanical energy density as well as the energy due to anisotropic switching between *a*-domain and *c*-domain are incorporated in the Hamiltonian. Besides, there are two contributions to the strain at each cell: eigenstrain and elastic strain. Our simulation results show that the longitudinal strain-electric field butterfly loop shifts downward along strain axis and that for the transverse strain shifts upward as the stress magnitude is increased. Moreover, the polarization-electric field hysteresis loop becomes a double-loop under a large compressive stress. The piezoelectric coefficient increases with the stress magnitude and reaches a maximum value at a critical stress level. It then gradually decreases to a small value at large stress magnitudes. Our results qualitatively agree with experimental ones.

Introduction

Ferroelectric thin films, by virtue of their coupled electromechanical characteristics, have been widely recognized for their potential utility in a large number of micro-electromechanical systems (MEMS) applications, including high-frequency ultrasonic transducers, accelerometers, pumps, and motors [1, 2]. The suitability of ferroelectric materials for MEMS application depends on their inherent high dielectric and piezoelectric responses [3, 4]. Investigations have shown that their macroscopic response to mechanical and electrical loadings is strongly related to their microstructural domain configurations [5, 6]. The application of electric field or mechanical loading in excess of a critical magnitude can induce a dipole rotation inside a domain, which subsequently results in both ferroelectric and ferroelastic domain switching. In particular, non-180° domain switching is usually suggested as the origin for the enhanced macroscopic strain response in ferroelectric thin films. Consequently, a better understanding of the relationship between the domain configuration and the material properties can provide guidelines to optimize the electromechanical properties by manipulating the stress, which is crucial for the design of ferroelectric film-based electromechanical devices.

Some researchers have performed experimental investigations on the dielectric and piezoelectric response of ferroelectric materials under combined electro-mechanical loadings. Zhou and Kamlah [7] measured the polarization and strain responses of soft lead zirconate titanate piezoceramics under different combined electromechanical loading conditions. Significantly enhanced dielectric and piezoelectric performance was observed within a small prestress range. Chaplya et al. also presented that the influence of electro-thermo-mechanical conditions on the actuation capabilities of five commercial piezoelectric stack actuators. Their results indicate that strain output could be increased by 60% for some actuators upon the application of a certain uniaxial compressive prestress [8]. Recently,

H.-X. Cao (✉) · Z.-Y. Li
Department of Physics, Jiangsu Key Laboratory of Thin Films, Soochow University, Suzhou 215006, China
e-mail: hxcao@suda.edu.cn

H.-X. Cao · V. C. Lo
Department of Applied Physics, The Hong Kong Polytechnic University, Hong Kong, China

Duan et al. studied tetragonal $PbTiO_3$ under uniaxial stress along the c-axis from first-principles. They found that the uniaxial compressive stress could enhance the piezoelectric stress coefficients, whereas the uniaxial tensile stress could enhance the piezoelectric strain coefficients [9]. On the other hand, the dynamic piezoelectric response of ferroelectric materials is comprised of intrinsic (piezoelectric lattice strain) and extrinsic (non-180° domain wall motion) components. Various attempts have been carried out to explore the 90° domain switching contribution to the dynamic polarization and piezoelectric behavior in ferroelectric materials. One of the most notable examples is the endeavor by Burcsu et al. in which the strain induced by 90° domain switching in barium titanate single crystals under combined electrical and mechanical loadings was examined, and a strain of nearly 0.8% was observed under the combined loading condition of 1.78 MPa compressive stress and 1 MV m^{-1} electric field [10]. Besides, local strain analysis for a $BaTiO_3$ single crystal under electric loading was conducted using X-ray microdiffraction technique. During the polarization reversal, local 90° domain switching was observed and contributed to the local strain distributions [11]. Therefore, it is significantly crucial to investigate the domain switching process in the microscopic scale under coupled electromechanical loadings since 90° domain switching is not only strongly affected by applied stress but also related to the dielectric and piezoelectric properties of ferroelectric materials [12–14].

Although the electromechanical properties of ferroelectric thin films under the combined electrical and mechanical loadings have been extensively investigated by various experimental techniques [15–17], a number of important aspects of the nonlinear behavior, such as the mechanism of polarization switching and the effect of 90° domain switching on piezoelectric coefficients and strain, are still not well understood. Some researchers analyzed the mechanical effect by superimposing a coupling term between the strain and polarization in the Landau–Ginzburg (LG) theory [18–20]. As we know, the LG theory is a macroscopic phenomenological theory which cannot describe the detailed relation between the dipole and the strain in the microscopic scale. In addition, although q-state Potts model was introduced to investigate the dynamic hysteresis by Monte Carlo simulation [21, 22], the stress effect was not taken into consideration. Therefore, the main focus of this work is to investigate the role of stress on the domain configuration which influences the electromechanical properties in ferroelectric thin films. In a previous paper, we have successfully explored the dielectric and strain response of ferroelectric thin films by this approach [23]. However, the piezoelectric and strain response driven by combined electrical and uniaxial compressive loadings has never been tackled before. Thus, we will explore the impact of uniaxial compressive stress on the dynamic hysteresis, longitudinal and transverse strain, piezoelectric coefficients d_{33} and d_{31} of multi-domain ferroelectric thin films.

Modeling and simulation

In this paper, it is assumed that all physical properties only vary along the thickness direction while remaining uniform over the transverse (xy) plane. All kinetics along the y direction can be equally replaced by those along the x direction because of the invariance of ferroelectric properties along the transverse plane. Consequently, the ferroelectric thin film can be represented by a two-dimensional array of rectangles $N_x \times N_z$, where N_x and N_z are the numbers of rectangles along x (transverse) and z (thickness) directions, respectively. Each of the rectangles represents a perovskite cell in tetragonal phase lying on the x–z plane. The location of a rectangle in the film can be described by a pair of indices (i, j), where $0 < i \leq N_x$ and $0 < j \leq N_z$. The dipole of each cell can be denoted by a state variable, which is called a pseudo-spin matrix $\hat{S}_{ij}$. There are four possible states for the matrix: a ($+z$ direction), b ($+x$ direction), c ($-z$ direction), and d ($-x$ direction). The explicit values for these states in matrix form are

$$\hat{S}_{ij} = \begin{pmatrix} 1 \\ 0 \end{pmatrix} (\text{in state } a), \quad \hat{S}_{ij} = \begin{pmatrix} 0 \\ 1 \end{pmatrix} (\text{in state } b),$$
$$\hat{S}_{ij} = \begin{pmatrix} -1 \\ 0 \end{pmatrix} (\text{in state } c), \quad \hat{S}_{ij} = \begin{pmatrix} 0 \\ -1 \end{pmatrix} (\text{in state } d). \tag{1}$$

The Hamiltonian of the system can be expressed as

$$H = -\sum_{\langle ij,km \rangle} J_0 \hat{S}_{ij}^{\mathrm{T}} \hat{S}_{km} - \sum_{ij} p_0 \hat{E}^{\mathrm{T}} \hat{S}_{ij} - \sum_{ij} \hat{\sigma}^{\mathrm{T}} \hat{\varepsilon}_{ij} + H', \tag{2}$$

where the superscript T indicates transposition of a matrix. In Eq. 2, the first term corresponds to the interaction of nearest-neighboring dipoles, where J_0 is the coupling coefficient through nearest-neighboring dipole–dipole interaction. The second term represents the coupling energy between the dipole and the external field, where p_0 is the magnitude of the dipole moment in one perovskite cell. The electric field $\hat{E}$ can be denoted by a column matrix such that

$$\hat{E} = \begin{pmatrix} E_z \\ E_x \end{pmatrix}, \tag{3}$$

where E_z and E_x are the components along z and x directions, respectively. In this paper, we only concentrate on the case of the external field along z direction $E_z = E_m \sin(2\pi t/\Gamma)$, $E_x = 0$, where t is the time and Γ the period. The third term corresponds to the coupling

energy between the stress $\hat{\sigma}_{ij}$ and the strain $\hat{\varepsilon}_{ij}$. The stress state $\hat{\sigma}_{ij}$ can be represented as the following matrix:

$$\hat{\sigma}_{ij} = \begin{pmatrix} \sigma_{\mathrm{l}} \\ \sigma_{\mathrm{t}} \end{pmatrix}, \tag{4}$$

where σ_{l} is the component normal to the film surface and σ_{t} tangential to the surface. We only consider the uniaxial stress in this paper ($\sigma_{\mathrm{t}} = 0$). $\hat{\varepsilon}_{ij}$ denotes the strain state of each cell, which is composed of two parts: the eigenstrain $\hat{\varepsilon}_{ij}^{\mathrm{eigen}}$ and the elastic strain $\hat{\varepsilon}_{ij}^{\mathrm{elastic}}$. The eigenstrain $\hat{\varepsilon}_{ij}^{\mathrm{eigen}}$ can be written as

$$\hat{\varepsilon}_{ij}^{\mathrm{eigen}} = \begin{pmatrix} \varepsilon_0 \\ -\varepsilon_0/2 \end{pmatrix} (\text{in state } a \text{ or } c) \quad \text{and}$$
$$\hat{\varepsilon}_{ij}^{\mathrm{eigen}} = \begin{pmatrix} -\varepsilon_0 \\ \varepsilon_0/2 \end{pmatrix} (\text{in state } b \text{ or } d), \tag{5}$$

where ε_0 is the magnitude of longitudinal eigenstrain in the unit cell. Li and Weng [24] have also suggested a similar association between the polarization direction and the eigenstrain state. The eigenstrain is associated with the switching of dipole. The elastic strain $\hat{\varepsilon}_{ij}^{\mathrm{elastic}}$ can be expressed as follows:

$$\hat{\varepsilon}_{ij}^{\mathrm{elastic}} = \frac{1}{Y}\begin{pmatrix} 1 & -v \\ -v & 1 \end{pmatrix}\begin{pmatrix} \sigma_{\mathrm{l}} \\ \sigma_{\mathrm{t}} \end{pmatrix}, \tag{6}$$

where v and Y are Poisson ratio and Young's modulus, respectively. The fourth term H' represents the anisotropic switching effect, which represents the inequality in probabilities (or energy) for a dipole switching from a longitudinal orientation to a transverse one, and vice versa. Recently, experimental research has confirmed the domain switching anisotropy in poled lead titanate zirconate ceramics under electromechanical loadings [25]. H' can be expressed as

$$H' = -\sum_{ij} w(\phi_c - \phi_a)\left|\hat{n}^{\mathrm{T}}\hat{S}_{ij}\right|, \tag{7}$$

where ϕ_c represents the switching anisotropy parameter and $\phi_a = 1 - \phi_c$, w is the energy barrier between a- and c-domains, $\hat{n}^{\mathrm{T}}$ is the transpose matrix of the unit matrix $\hat{n} = \begin{pmatrix} 1 \\ 0 \end{pmatrix}$.

In our simulation, periodic boundary condition is chosen for the pseudo-spins at the transverse edges and free boundary condition for both the top and bottom surfaces. The initialization of pseudo-spins has been described previously [26]. Only the dipoles at the domain walls [2] are allowed to rotate by a 90° rotation, either along clockwise or counterclockwise direction. This rotation is associated with the distortion of cell, which can be described by the eigenstrain states, as expressed in Eqs. 1 and 5. Consequently, a dipole at the domain walls is randomly selected. Whether it is allowed to rotate or not is determined by the Metropolis algorithm as described previously [26].

On the other hand, in order to simulate a time-dependent process, the number of computational steps must be scaled with some characterization time of the system. Considering an initially unpoled system subject to a positive dc field, dipoles inside the film rotate sequentially. The overall polarization gradually increases until it finally attains a steady-state value. The switching time is then defined as the time required to achieve 99% of the steady-state value. It can be shown that this switching time should be independent of the selection of the grid size for the system. In our simulation, the relation between the Monte Carlo step t_{MCS} and physical time t_{real} can be expressed as

$$t_{\mathrm{MCS}} = t_{\mathrm{real}}\frac{N_x N_z}{\Delta t}. \tag{8}$$

where Δt is the infinitesimally small time step. The external alternating electric field can then be expressed as

$$E_z = E_0 \sin\left(\frac{2\pi t}{\Gamma}\right) = E_0 \sin\left(\frac{2\pi t_{\mathrm{MCS}}}{\Gamma_{\mathrm{MCS}}}\right), \tag{9}$$

where $\Gamma_{\mathrm{MCS}} = \Gamma_{\mathrm{real}}(N_x N_z)/\Delta t$.

The polarization can be calculated by the ensemble average of the system, such that

$$P_z = \frac{\sum_{i,j}\left\{\hat{S}_{ij}^{\mathrm{T}} \times \hat{n}\right\}}{N_x N_z}. \tag{10}$$

The longitudinal strain ε_{l} and the transverse strain ε_{t} are evaluated by

$$\varepsilon_{\mathrm{l}} = \frac{1}{N_x N_z}\sum_{ij} \hat{n}^{\mathrm{T}}\left(\hat{\varepsilon}_{ij} - \hat{\varepsilon}_{ij}^0\right), \tag{11}$$

$$\varepsilon_{\mathrm{t}} = \frac{1}{N_x N_z}\sum_{ij} \hat{q}^{\mathrm{T}}\left(\hat{\varepsilon}_{ij} - \hat{\varepsilon}_{ij}^0\right), \tag{12}$$

where $\hat{\varepsilon}_{ij}^0$ is the initial strain matrix for each cell, and $\hat{q} = \begin{pmatrix} 0 \\ 1 \end{pmatrix}$ is the unit matrix along the transverse direction.

The piezoelectric coefficients, d_{33} and d_{31}, are approximately calculated by

$$d_{33} = \left.\frac{\Delta\varepsilon_{\mathrm{l}}}{\Delta E_z}\right|_{E_z=0}, \tag{13}$$

$$d_{31} = \left.\frac{\Delta\varepsilon_{\mathrm{t}}}{\Delta E_z}\right|_{E_z=0}. \tag{14}$$

The calculated d_{33} and d_{31} are nearly equal to the slopes of the $\varepsilon_{\mathrm{l}} - E_z$ and $\varepsilon_{\mathrm{t}} - E_z$ curves as the electric field passes through zero.

Results and discussion

In our simulation, we have adopted the following numerical parameters: $\Gamma = 400$, $E_0 = 1.5$, $T = 1.2$, $\varepsilon_0 = 0.5$, $w = 0.8$, $Y = 2.0$, $v = 0.3$, $\phi_c = 0.6$, $N_x = 150$, and $N_z = 80$. We have systematically discussed the impact of stress on the polarization and dielectric properties of ferroelectric thin films using this set of dimensionless parameters, which can be used to explain the generic electromechanical behaviors found in perovskite oxides [23].

It is a well-known fact that the nonlinear behavior of ferroelectric thin films can be attributed to the polarization switching through the domain wall movements. If it is possible to analyze hysteresis loop in details, all information about domain switching behavior can be obtained exactly. A series of the polarization versus electric field hysteresis (or *P–E*) loops under different uniaxial compressive stress values ($\sigma_1 = -0.4, -0.8, -1.4, -1.6$) are plotted in Fig. 1. For small stress magnitudes, ($\sigma_1 = -0.4, -0.8$), both the remanent polarization and the coercive field are reduced, which can be attributed to the depolarization induced by mechanical loading through 90° ferroelastic domain switching process. This is accompanied by an earlier start and later ending of the switching process, which is also called "soft" switching behavior, in analogy to ferromagnetic materials. The uniaxial compressive stress forces more domains to be reoriented perpendicular to the electric field so as to contribute to the polarization switching. The slope of the *P–E* hysteresis loop at zero electric field, which represents the permittivity of the ferroelectric thin films in the remanent state, increases with the increase of the compressive stress. On increasing the stress magnitude, the hysteresis loop becomes "slim" and the loop area shrinks, which is directly related to the amount of domains participating in the switching process over a cycle. It is clear that the amount of domains participating in polarization switching decreases when the stress magnitude is larger than a critical value. Moreover, for large compressive stress, the hysteresis loop has the double-loop feature ($\sigma_1 = -1.4$, and -1.6). Both the remanent polarization and coercive field are reduced to zero. It can be understood that the large uniaxial compressive stress suppress the polarization along z direction, and only an exceeding large electric field can switch the dipole. In particular, in the case of large compressive stress (σ_1), only a very large external field can align dipoles along z direction and the loop area obviously shrinks, which implies that relatively few domains participate in polarization reversal under such a high stress loading. Similar phenomenon has been observed by Granzow et al. [27], from the impact of defect structure on the polarization and strain response of iron-doped lead zirconate titanate. This effect can be explained by the introduction of extra oxygen vacancies. Although the physical reasons for the phenomena are different, both the cases are strongly associated with the domain switching process.

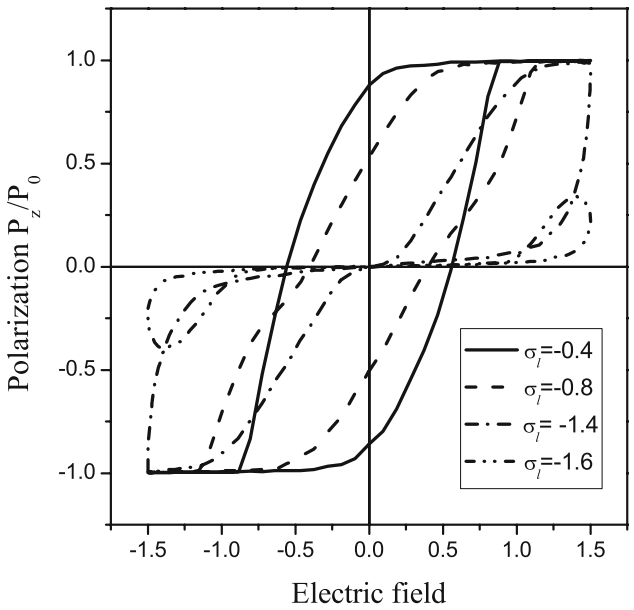

Fig. 1 The polarization versus electric field hysteresis loops under different uniaxial compressive stresses ($\sigma_1 = -0.4, -0.8, -1.4, -1.6$)

The butterfly loops for longitudinal strain ε_l and transverse strain ε_t versus electric field at various magnitudes of uniaxial compressive stress are shown in Fig. 2a and b, respectively. The numeric labels in these figures are the stress values. The solid and dash lines are the simulation results taking into account the contribution of elastic strain and those without the contribution of elastic strain, respectively, under a given compressive stress σ_1. Similar butterfly loop can be found in Ref. [28], which demonstrated the effect of uniaxial preload stress on the ferroelectric hysteretic response of soft lead zirconate titanate. One of the most notable features from these loops is that $\varepsilon_l - E_z$ loop shifts toward the negative strain direction and $\varepsilon_t - E_z$ shifts toward the opposite direction as the stress level increases. For instance, at a given compressive stress $\sigma_1 = -0.4$, $\varepsilon_l - E_z$ curve shifts to the negative strain direction if the elastic strain contribution is considered. Besides, we have found that the longitudinal (transverse) strain-electric field loop does not shift along the strain axis while neglecting the contribution of elastic strain. Here, we only show the results with and without the elastic strain for the given compressive stress $\sigma_1 = -0.4$ in order to compare with those without the elastic stress. As pointed out by Lynch [29], there are two different contributions of strains in response to the applied stress. The first one is the eigenstrain, i.e. the deformation of a perovskite cell is

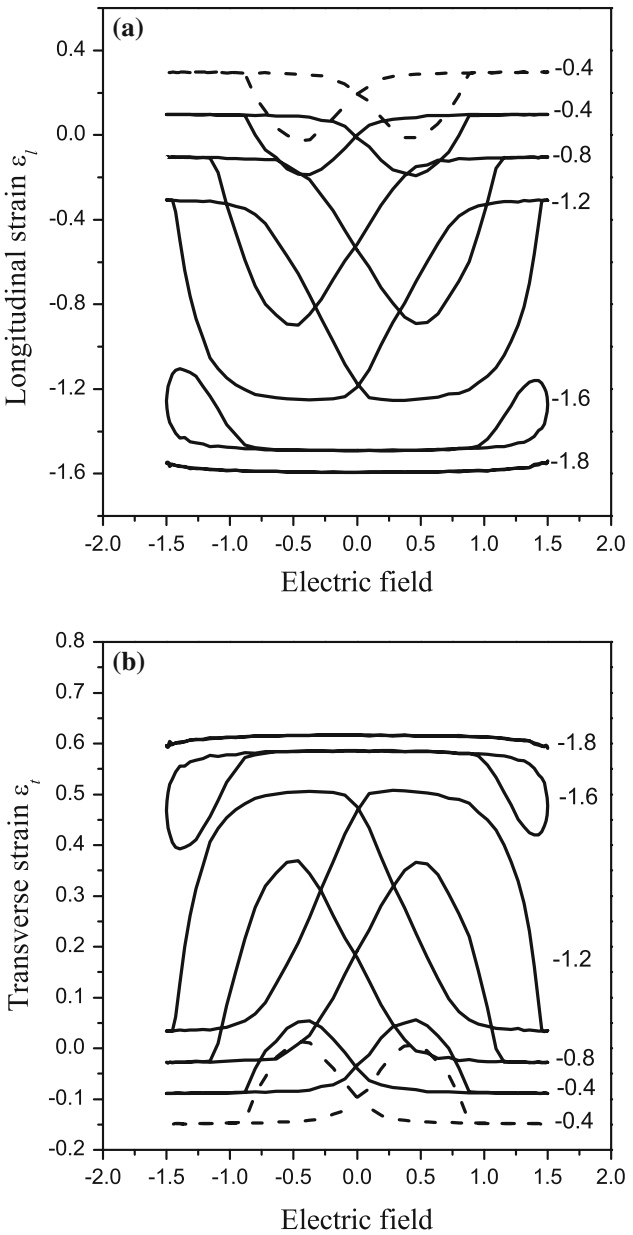

Fig. 2 The longitudinal strain ε_l (**a**) and transverse strain ε_t (**b**) versus electric field butterfly-type hysteresis loop curves at various stress levels. The numeric labels are values of compressive stresses

associated with the rotation of dipole so that there is a connection between the strain states and the dipole states of the cell. This contribution is accountable to formation of the butterfly loop. The second one is the elastic deformation, which is merely the mechanical property of material. The contribution of elastic strain results in the vertical shift of the butterfly loop. Therefore, the elastic strain should be taken into consideration. The loop area for both longitudinal and transverse strains is gradually enlarged on increasing the compressive stress, and attains a maximum loop area when the stress value is about -1.2. This indicates that the strain amplitude $\Delta\varepsilon_l$ between the maximum and minimum value of strain ε_l has a maximum value while $\sigma_1 = -1.2$. The loop area then gradually shrinks and finally reduces to a horizontal line at a very large stress value ($\sigma_1 = -1.8$). In general, the longitudinal compressive stress induces the dipoles to be preferentially aligned along the film (both states *b* and *d*), but the longitudinal electric field drives them to switch to energetically favorable states, either state *a* or *c*. The switching of dipole results in a large deformation of the sample because of a larger change in ferroelastic strain. Under a small compressive stress, the competition between the longitudinal compressive stress and longitudinal electric field not only enlarges the butterfly loop area, but also broaden the loop to the large magnitude of electric field. However, under a large compressive stress ($\sigma_1 = -1.6$), only a very large electric field can switch the dipole. Consequently, a small loop appears at a large field magnitude while there is no change in strain when the field magnitude is small. This means the strain changes only if the external field exceeds a certain value. The clamping the dipoles along the transverse plane at small electric field and large compressive stress explains this double-loop feature. This behavior is also reflected by the hysteresis loop, as shown in Fig. 1. With further increase in the compressive stress, all dipoles are clamped along the transverse direction and the switching is difficult. The loop area then becomes smaller and is finally constricted to a horizontal line. It can be concluded that the elastic strain plays a crucial role in the vertical shift of strain-external field butterfly loop. Our theoretical results are in good agreement with the experimental ones [28], which revealed that the superimposed compression load had a significant impact on the longitudinal/transverse strain-electric field response under combined electromechanical loadings.

On the other hand, both the stress-induced ferroelastic domain switching and stress clamping play a crucial role in the piezoelectric performance of ferroelectric films. Many experimental investigations have focused on the dependence of piezoelectric behavior of ferroelectric materials on the uniaxial stress. For instance, the effect of uniaxial compressive stress on the piezoelectric coefficients d_{33} and d_{31} in lead zirconate titanate has been experimentally investigated by Zhao and Zhang [30], where the piezoelectric coefficients showed a non-linear behavior with a initial increase in d_{33} and d_{31} as the stress increases followed by a significant decrease. In order to compare with the experimental results, Fig. 3a and b displays the uniaxial compressive stress dependence of piezoelectric coefficient d_{33} and d_{31}. The magnitudes of piezoelectric coefficient d_{33} and d_{31} initially increase with the stress magnitude, reaching the peak values at a critical stress. Thereafter, the magnitudes of d_{33} and d_{31} decrease quickly on further increasing the stress magnitude and finally approach zero,

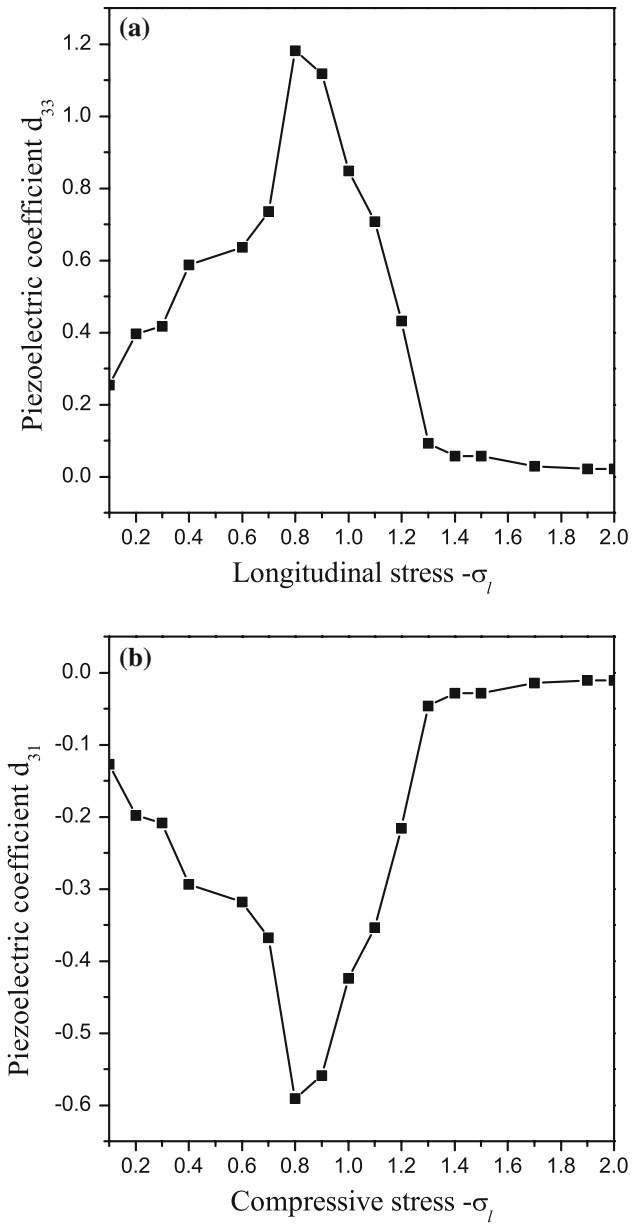

Fig. 3 The uniaxial compressive stress dependence of piezoelectric coefficient d_{33} (**a**) and d_{31} (**b**)

which indicates that there is hardly any piezoelectric effect under such high compressive stress loading. This well agrees with the experimental results [28, 30].

Conclusion

In summary, we have developed a modified planar four-state Potts model to investigate the electromechanical properties in the ferroelectric thin films under an alternating electric field and static uniaxial compressive stress. We introduce the coupling interaction energy between the strain and the stress, as well as the anisotropic domain switching energy between *a*-domain and *c*-domain into the Hamiltonian. Besides, the strain can be divided into eigenstrain and elastic strain. By use of the Monte Carlo simulation, the influence of uniaxial compressive stress on the hysteresis loop, butterfly loops for longitudinal and transverse strains, and piezoelectric coefficients is analyzed. We have shown that uniaxial compressive stress can not only reduce the remanent polarization but also reduce the coercive field for a small compressive stress. Then, the two-loop feature occurs in the case of large compressive stress. Besides, the vertical shift for longitudinal and transverse butterfly strain-external field is simulated. Furthermore, the piezoelectric coefficient d_{33} and d_{31} reach the peak values at a specific uniaxial compressive stress. These results indicate that both the uniaxial compressive stress and the domain configuration have a significant influence on the electromechanical performance of the ferroelectric thin films. Our results are in good agreement with the experimental ones.

Finally, it should be noted that the internal strains arising from the lattice mismatch and the thermal expansion mismatch between the film and the substrate also play a significant role in the electromechanical properties of ferroelectric films in addition to the external loading. Especially, in-plane anisotropic misfit strain may appear for the film grown on a dissimilar tetragonal or orthorhombic substrate. These strains determine the domain distribution for the multi-domain film. Therefore, we will develop a Monte Carlo algorithm based on the three-dimensional *q*-state Potts model to deal with the technologically important multi-domain ferroelectric ceramics, taking into account both the internal misfit strains and external loading.

Acknowledgements This work was supported by the Research Grant of the Hong Kong Polytechnic University under the Grant No. 1-ZV44, the National Natural Science Foundation of China under the Grant Nos. 10474069 and 50832002, the Natural Science Foundation of JiangSu Education Committee of China under the Grant No. 08KJB140006. One of authors, H.X. Cao, was supported by the Jiangsu Government Scholarship for Overseas Studies.

References

1. Zhou QF, Zhang QQ, Yoshimura T et al (2003) Appl Phys Lett 82:4767
2. Zhao P, Li J (2008) J Appl Phys 103:104104
3. Tan X, Jo W, Granzow T et al (2009) Appl Phys Lett 94:042909
4. Bell AJ (2006) J Mater Sci 41:13. doi:10.1007/s10853-005-5913-9
5. Grigoriev A, Do DH, Kim DM et al (2006) Phys Rev Lett 96:187601
6. Fu H, Bellaiche L (2003) Phys Rev Lett 91:057601
7. Zhou D, Kamlah M (2004) J Appl Phys 96:6634
8. Chaplya PM, Mitrovic M, Carman GP et al (2006) J Appl Phys 100:124111

9. Duan Y, Shi H, Qin L (2008) J Phys Condens Matter 20:175210
10. Burcsu E, Ravichandran G, Bhattacharya K (2004) J Mech Phys Solids 52:823
11. Park JH, Park J, Lee KB, Koo TY et al (2007) Appl Phys Lett 91:012906
12. Shieh J, Yeh JH, Shu YC et al (2007) Appl Phys Lett 91:062901
13. Jones JL, Hoffman M, Daniels JE et al (2006) Appl Phys Lett 89:092901
14. Osone S, Shimojo Y, Brinkman K et al (2007) Appl Phys Lett 90:262905
15. Achuthan A, Sun CT (2005) J Appl Phys 97:114103
16. Suchanicz J, Sitko D, Kim-Ngan NTH et al (2008) J Appl Phys 104:094106
17. Fu D, Suzuki K, Kato K (2003) Appl Phys Lett 82:2130
18. Budimir M, Damjanovic D, Setter N (2005) Phys Rev B 72:064107
19. Emelyanov AY, Pertsev NA, Kholkin AL (2002) Phys Rev B 66:214108
20. Yang G, Yue Z, Sun T et al (2008) J Phys D Appl Phys 41:045307
21. Liu JM, Chan HL, Choy CL (2002) Mater Lett 52:213
22. Liu JM, Lau ST, Chan HLW, Choy CL (2006) J Mater Sci 41:163. doi:10.1007/s10853-005-6016-3
23. Cao HX, Lo VC, Chung WWY (2006) J Appl Phys 99:024103
24. Li WF, Weng GJ (2002) J Appl Phys 91:3806
25. Li FX, Fang DN, Liu YM (2006) J Appl Phys 100:084101
26. Li KT, Lo VC (2005) J Appl Phys 97:034107
27. Granzow T, Suvaci E, Kungl H et al (2006) Appl Phys Lett 89:262908
28. Zhou D, Kamlah M, Munz D (2005) J Eur Ceram Soc 25:425
29. Lynch CS (1996) Acta Mater 44:4137
30. Zhao J, Zhang QM (1996) Proc ISAF IEEE Symp, p 971